A R C H I V E O F M E C H A N I C A L E N G I N E E R I N G

Volume 66 2019 Number 4

DOI: 10.24425/ame.2019.131354

Key words: thermal buckling, functionally graded material, transformed-section method, temperature-dependent properties

Wei-Ren Chen[1], Chun-Sheng Chen[2], Heng Chang[1]

Thermal buckling of temperature-dependent functionally graded Timoshenko beams

Thermal buckling behavior of a functionally graded material (FGM) Timoshenko beam is studied based on the transformed-section method. The material and thermal properties of the FGM beam are assumed to vary across the beam thickness according to a power-law function, a sigmoid function and an exponential function. The results of buckling temperature for the FGM beams with respective temperature-dependent and temperature-independent properties under uniform and non-linear temperature rises are presented. Some results are compared with those in the published literature to verify the accuracy of the present work. The effects of the material distributions, temperature fields, temperature-dependent properties and slenderness ratios on the thermal buckling behaviors of FGM beams are discussed. It is believed that the present model provides engineers with a simple and effective method to study the effects of various parameters of the FGM beam on its thermal buckling behavior.

1. Introduction

Functionally graded materials (FGMs) are non-traditional composite materials with a smooth variation of material properties in the specified directions. This graded property is achieved by gradually varying the volume fraction of the constituent materials so that the discontinuity of mechanical properties between materials can be eliminated. Generally, FGMs are made of the ceramic and metal with the properties of the high toughness of metal and excellent strength and temperature resistance of ceramic. Thus, engineering structures made from ceramic/metal FGMs have been widely used in many fields under thermal environments.

✉ W.-R. Chen, e-mail: wrchen@faculty.pccu.edu.tw

[1]Department of Mechanical Engineering, Chinese Culture University, Taipei, Taiwan.

[2]Department of Mechanical Engineering, Lunghwa University of Science and Technology, Guishan Shiang 33306, Taiwan.

When a structure is subjected to a high-temperature condition, under certain conditions the thermal buckling due to the thermal loading may occur. Therefore, a good understanding of the thermal buckling behavior of FGM structures, especially for beam members, in thermal conditions is needed in order to use them in an effective and safe way. The buckling problems [1–14] of FGM beams subjected to mechanical loads had been studied in the past decades by various analytical and approximate methods. Because the present paper is focused on the study of thermal buckling of FGM beams, merely the relevant literature is reviewed next.

In [15] authors presented close-form expressions for the critical thermal buckling temperature of FGM Euler-Bernoulli beams under various thermal loadings. The material properties are assumed to vary across the thickness direction according to a power-law function. The effects of temperature distributions such as uniform temperature rise, linear and nonlinear temperature distribution on the thermal buckling were investigated. In [16] authors studied the thermal buckling and free vibration of third-order shear deformable FGM beams subjected to uniform temperature rise. The effects of material compositions, power law indices, slenderness ratios, temperature-dependent properties and boundary conditions were investigated. The results indicated that temperature-dependent properties significantly affect the thermal buckling and vibration of the thick beams. Based on the Galerkin's decomposition method [17], authors investigated the thermo-mechanical buckling and non-linear vibration of FGM Euler-Bernoulli beams on non-linear elastic foundations. A simple power law is used to model the smooth change of material properties in the thickness direction. Closed-form solutions for the critical buckling temperature and nonlinear natural frequency were established and used to study the effects of volume fraction indices, foundation parameters, thermal loads, vibration amplitudes and boundary condition. In [18] authors analyzed the thermal-mechanical buckling of temperature-dependent FGM Timoshenko beams using the virtual displacements principle. The material and thermal properties are changed across the thickness with a power-law distribution, and depend on temperature and position. Close-form solutions were obtained for the critical thermal buckling temperature of FGM beams under uniform temperature rise, linear and nonlinear temperature distribution, respectively. In [19] authors presented the critical buckling temperature and buckling modes of FGM Timoshenko beams with longitudinal crack under uniform temperature rise using the Hamilton's principle and differential quadrature method. The materials properties are varied along the thickness direction according to a power law distribution. The effects of material graded index, crack length, crack depth and crack position were discussed. Based on the Ritz method [20], the authors investigated the thermal buckling and post-buckling behaviors of temperature-dependent FGM Timoshenko beams under uniform temperature rise and heat conduction using a generalized differential quadrature method. The properties are assumed to vary across the thickness direction by a simple power law function. The effects of the power-law index, foundation stiffness, thermal loading types, temperature-dependent properties and boundary

conditions on thermal stability behaviors were studied. In [21] authors applied the Hamilton's principle and state space approach to analyze the vibration and buckling behaviors of higher order shear deformable FGM beams under mechanical and thermal loads. The material properties are assumed to depend on the temperature and position, and vary along the thickness according to a power law function. Three types of thermal loadings such as uniform, linear and nonlinear temperature rise were taken into account. The effects of material constituents, power law indices, temperature distributions, slenderness ratios and restraint conditions on the buckling temperature, buckling loads and natural frequencies were discussed. Based on a shooting method [22], authors presented the thermal buckling and post-buckling of FGM Timoshenko beams with properties varying along the thickness by a power law function. The beam is assumed to rest on non-linear elastic foundations and be subjected to uniform and non-linear temperature rise, respectively. The influences of the foundation stiffness, power law exponent and slenderness ratio on the buckling temperature and post-buckling deformations were investigated. In [23] authors investigated the hygro-thermal effects on the vibration and thermal buckling of high order shear deformable FGM beams using Lagrange's equations and Ritz method. The effects of power law index, slenderness ratio, transverse normal strain, temperature and moisture on natural frequencies and buckling temperatures were examined. In [24] authors studied thermal buckling and post-buckling behaviors of FGM beams under uniform temperature rise using the Euler–Bernoulli, Timoshenko and various higher-order shear deformation beam theories. The temperature-dependent properties of the constituents were considered. A two-step perturbation method was used to obtain the buckling loads and post-buckling equilibrium paths. In [25] authors investigated the thermal buckling of elastically supported FGM Timoshenko beams under uniform temperature rise using Stokes' transformation technique. Material properties are assumed to vary along the thickness direction according to a simple four-parameter power law. The effects of the power law index, FGM model, slenderness ratio and restraint conditions were examined. Based on the variational principle and Ritz method [26], the authors presented the thermal buckling stability of fixed-fixed FGM Euler-Bernoulli beams subjected to linear and nonlinear temperature gradient. The temperature-dependent material properties are assumed to vary along the thickness direction according to a power law function. The effects of material constituents, volume fraction index and slenderness ratio on the thermal buckling loads were investigated. In [27] authors investigated the thermal-mechanical buckling of porous FGM sandwich beams under thermal conditions based on the high order shear deformation theory and physical neutral plane. The temperature-dependent properties are approximated by a modified Voigt mixture rule. The effects of porosity, the physical neutral plane, gradient index, temperature-dependent properties, face-to-core ratios on the thermal buckling of porous FGM beams under uniform, linear and nonlinear temperature rises were examined.

As reviewed previously, most studies on thermal buckling problems were concentrated on FGM beams with material properties varying in the thickness direction

according to a power law function. Accordingly, various analytical and numerical methods were used to analyze FGM beam structures with good accuracy. However, the thermal buckling of FGM beams with the variation of material properties by a sigmoid function and an exponential function had seldom been reported. In addition, no attempt was made to analyze the thermal buckling problem of FGM Timoshenko beams based on the transformed-section method [28]. Thus, the present paper applies the transformed-section method [29, 30] to investigate the thermal buckling behaviors of FGM Timoshenko beams with material properties varying according to the power-law function (P-FGM), sigmoid function (S-FGM) and exponential function (E-FGM), respectively. The material and thermal properties of the beam are assumed to depend on the temperature and thickness coordinate. The temperature-dependent and temperature-independent solutions of the critical buckling temperatures for various clamped-clamped P-FGM, S-FGM and E-FGM beams under uniform temperature rise (UTR) and nonlinear temperature rise (NTR) are determined. To validate the accuracy of the present model, some calculated results for the critical buckling temperatures of FGM beams with various material models, volume fraction indices, temperature distributions and slenderness ratios are compared with those by other investigators. A good agreement is achieved. The effects of the material distribution types, temperature fields, volume fraction indices, temperature-dependent properties and slenderness ratios on the thermal buckling behaviors of different FGM beams are investigated.

2. Functionally graded materials

A FGM beam made from metal and ceramic is investigated, which has a length of l and rectangular cross-section of $b \times h$. The top surface of the beam is ceramic-rich and its bottom one is metal-rich. Fig. 1 shows the beam configuration and coordinate frames xyz and $x_1y_1z_1$. The axis x is on the physical midplane xy and the x_1 axis is the neutral axis of the transformed cross-section. The y and y_1 axes are in the width direction of the beam; the z and z_1 axes are collinear and along the thickness direction. The effective properties $P(z)$ of the FGM beam, such as the effective Young's modulus E, shear modulus G, thermal expansion coefficient α and thermal conductivity K, are assumed to change continuously across the beam

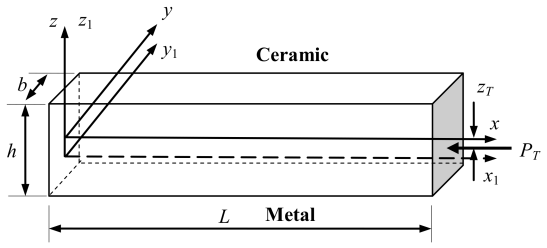

Fig. 1. Beam configuration and coordinate systems

thickness according to the power-law function, sigmoid function or exponential function.

For the P-FGM beam, its effective property is expressed as

$$P(z) = P_b + (P_t - P_b)\left(\frac{z}{h} + \frac{1}{2}\right)^k. \tag{1}$$

Here P_t and P_b represent the material properties of the beam at its upper and bottom surfaces, respectively; the non-negative exponent k is the volume fraction index; the thickness variable z ranges from $-h/2$ to $h/2$. Fig. 2 depicts the variation of property $P(z)/P_t$ in the thickness direction for the P-FGM beam with various values of k. As can be seen, a smaller value of volume fraction index represents a more sudden increase in the property $P(z)/P_t$ near the bottom surface and the material at the top surface is the dominant constituent. In contrast, the property $P(z)/P_t$ changes abruptly near the top surface for a larger value of volume fraction index and the dominant constituent is the material at the bottom surface. For S-FGM beam, its effective property $P(z)$ is expressed by two power law functions as follows.

$$P(z) = P_b + \frac{1}{2}(P_t - P_b)\left(1 + \frac{2z}{h}\right)^k, \qquad -h/2 \leqslant z \leqslant 0, \tag{2a}$$

$$P(z) = P_b + (P_t - P_b)\left[1 - \frac{1}{2}\left(1 - \frac{2z}{h}\right)^k\right], \qquad 0 \leqslant z \leqslant h/2. \tag{2b}$$

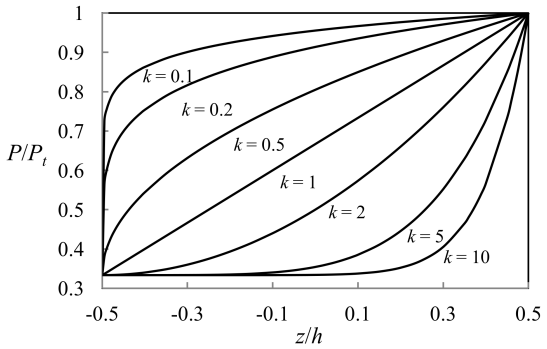

Fig. 2. Variation of effective property $P(z)/P_t$ versus beam thickness for P-FGM beam with various values of volume fraction index k

Fig. 3 shows the variation of property $P(z)/P_t$ against the thickness coordinate for the S-FGM beam with different values of k. It is noted that the property varies rapidly near the top and bottom surfaces for $k < 1$ but changes abruptly near the middle surface for $k > 1$. The effective property $P(z)$ for E-FGM beam is given as

$$P(z) = P_t e^{\gamma\left(\frac{2z}{h} - 1\right)}, \qquad \gamma = \frac{1}{2}\ln\left(\frac{P_t}{P_b}\right). \tag{3}$$

Fig. 4 illustrates the property $P(z)/P_t$ with respect to the thickness for the E-FGM beam. Like the P-FGM beam, the bottom surface is fully metal whereas the top surface is fully ceramic. Compared to Fig. 2, it is noted that its property falls between those of the P-FGM beam with $k = 1$ and 2.

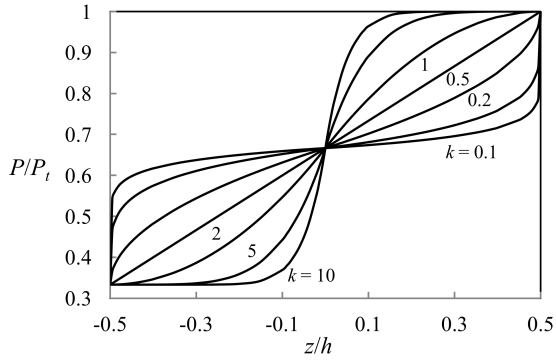

Fig. 3. Variation of effective property $P(z)/P_t$ versus beam thickness for S-FGM beam with various values of volume fraction index k

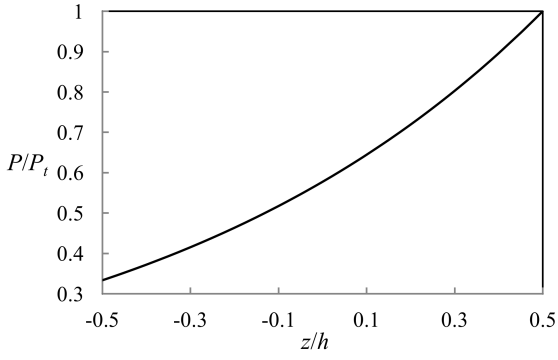

Fig. 4. Variation of effective property $P(z)/P_t$ versus beam thickness for E-FGM beam

When the materials considered are dependent on temperature, the nonlinear equation of the Touloukian model [31] is used to evaluate the thermal-elastic material properties in terms of temperature.

$$P = P_0 \left(P_{-1}T^{-1} + 1 + P_1 T + P_2 T^2 + P_3 T^3\right), \tag{4}$$

where P_0, P_{-1}, P_1, P_2 and P_3 are coefficients associated with the constituent and $T = T_0 + \Delta T$. T_0 and ΔT denote the ambient temperature (300 K) and temperature difference, respectively.

3. Temperature fields

In the present study, the temperature rise is assumed to vary along the thickness direction of the FGM beam. Additionally, the uniform temperature rise and nonlinear temperature rise thermal conditions are considered. For FGM beams subjected to uniform temperature rise, the temperature of the whole beam is uniform. The temperature change of the beam is $\Delta T = T - T_0$, in which T is the final temperature and $T_0 = 300$ K is the initial uniform temperature.

For FGM beams under nonlinear temperature rise, the temperature field $T(z)$ along the thickness can be obtained by solving the one-dimensional steady state heat conduction equation with the prescribed temperature conditions at the top and bottom surface

$$\begin{gathered} \frac{\mathrm{d}}{\mathrm{d}z}\left(K(z)\frac{\mathrm{d}T}{\mathrm{d}z}\right) = 0, \\ T\left(\frac{h}{2}\right) = T_t\,, \qquad T\left(-\frac{h}{2}\right) = T_b\,, \end{gathered} \tag{5}$$

where $K(z)$ is the thermal conductivity independent of the temperature, which can be obtained for the P-FGM, S-FGM and E-FGM beam from Eqs. (1) to (3), respectively. T_t and T_b represent the prescribed temperature at the top and bottom side, respectively. Then, substituting the expression of $K(z)$ into Eq. (5) and performing the integration, the temperature field for the P-FGM, S-FGM and E-FGM beam can be determined.

For P-FGM and S-FGM beams, the solution of Eq. (5) can be found by using the polynomial series. The temperature field for the P-FGM beam is given as [21]

$$T(z) = T_b + \frac{R_2}{R_1}\Delta T, \tag{6}$$

with

$$\begin{aligned} R_1 &= \sum_{j=0}^{n} \frac{(-1)^j}{(jk+1)}\bar{K}^j, \\ R_2 &= \sum_{j=0}^{n} \frac{(-1)^j}{(jk+1)}\bar{K}^j \left(\frac{z}{h} + \frac{1}{2}\right)^{jk+1}. \end{aligned}$$

The temperature distribution for the S-FGM beam is obtained as

$$T(z) = \begin{cases} T_b + \dfrac{D_2}{D_1}\Delta T & -h/2 \leqslant z \leqslant 0, \\ T_t - \dfrac{D_4}{D_3}\Delta T & 0 \leqslant z \leqslant h/2, \end{cases} \tag{7}$$

with

$$D_1 = \sum_{j=0}^{n} \frac{1}{(jk+1)} \left[\left(-\frac{1}{2}\bar{K} \right)^j + \frac{K_b}{K_t} \left(\frac{1}{2}\bar{K}_1 \right)^j \right],$$

$$D_2 = \sum_{j=0}^{n} \frac{(-1)^j}{(jk+1)} \left(\frac{1}{2}\bar{K} \right)^j \left(1 + \frac{2z}{h} \right)^{jk+1},$$

$$D_3 = \sum_{j=0}^{n} \frac{1}{(jk+1)} \left[\frac{K_t}{K_b} \left(-\frac{1}{2}\bar{K} \right)^j + \left(\frac{1}{2}\bar{K}_1 \right)^j \right],$$

$$D_4 = \sum_{j=0}^{n} \frac{1}{(jk+1)} \left(\frac{1}{2}\bar{K}_1 \right)^j \left(1 - \frac{2z}{h} \right)^{jk+1}.$$

Here $\Delta T = T_t - T_b$ is the temperature difference between the upper and bottom surfaces of the FGM beam; $\bar{K} = (K_t - K_b)/K_b$ and $\bar{K}_1 = (K_t - K_b)/K_t$. Sufficient terms of the series should be taken in evaluating the temperature distribution to ensure the convergence. For the E-FGM beam, the solution of Eq. (5) can be determined by direct integration. Its temperature field is given as

$$T(z) = T_b + \frac{\left(e^{-\gamma\left(\frac{2z}{h}-1\right)} - e^{2\gamma} \right)}{(1 - e^{2\gamma})} \Delta T. \tag{8}$$

4. Governing equations

Considering a FGM beam subjected to the temperature rise from the reference temperature T_0 to the current temperature T, it can be regarded as a beam under a thermal compressive load P_T at a distance z_T as given in Fig. 1. They can be determined as follows:

$$P_T = -\int E(z)\alpha(z)\,(T - T_0)\,\mathrm{d}A, \tag{9}$$

$$z_T = \frac{\int E(z)\alpha(z)z\,(T - T_0)\,\mathrm{d}A}{\int E(z)\alpha(z)\,(T - T_0)\,\mathrm{d}A}. \tag{10}$$

Here $E(z)$ and $\alpha(z)$ are the effective Young's modulus and thermal expansion coefficient, respectively. They can be obtained for the respective P-FGM, S-FGM and E-FGM beam according to Eqs. (1) to (3).

In deriving the differential equations governing the bending defection of the FGM beam under a thermal compressive load using the transformed-section method, the original rectangular cross section (Fig. 5a) of FGM beam with two

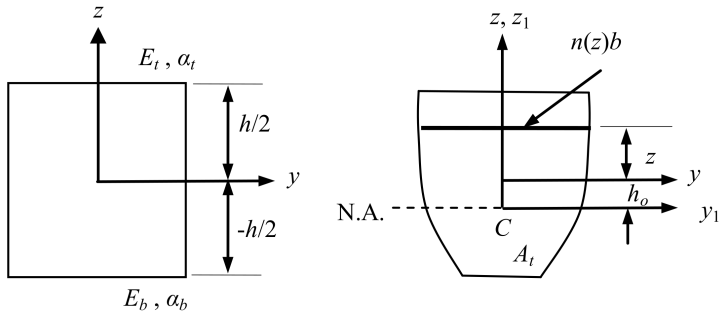

(a) original section (b) transformed section

Fig. 5. Beam of functionally graded materials

compositions is transformed into an equivalent cross-section with the material of the top surface (Fig. 5b). A modular ratio, $n(z)$, is defined as

$$n(z) = \frac{E(z)}{E_t}\,. \tag{11}$$

Then, the centroid of the neutral axis of the transformed section, h_o, the cross-sectional area of transformed section, A_t, and the effective second moment of area about the neutral axis of this transformed area, I_e, are obtained as

$$h_o = \frac{\int\limits_{A_t} z\,\mathrm{d}A}{\int\limits_{A_t} \mathrm{d}A} = \frac{\int\limits_{-h/2}^{h/2} zn(z)b\,\mathrm{d}z}{\int\limits_{-h/2}^{h/2} n(z)b\,\mathrm{d}z}, \tag{12}$$

$$A_t = \int\limits_{-h/2}^{h/2} bn(z)\,\mathrm{d}z, \tag{13}$$

$$I_e = \int\limits_{A_t} z_1^2\,\mathrm{d}A = \int\limits_{-h/2}^{h/2} bn(z)z^2\,\mathrm{d}z - h_o^2 \int\limits_{-h/2}^{h/2} bn(z)\,\mathrm{d}z. \tag{14}$$

The detailed derivations of Eqs. (12)–(14) can be found in the authors' earlier work [29, 30]. Introducing the expression of $E(z)$ into Eqs. (11) to (14), we can obtain the modular ratio, centroid, area of transformed section and effective area moment of inertia for the respective P-FGM, S-FGM and E-FGM beam as follows.

P-FGM:

$$n(z) = \bar{E} + \left(1 - \bar{E}\right)\left(\frac{z}{h} + \frac{1}{2}\right)^k, \tag{15a}$$

$$h_o = \frac{k\left(1 - \bar{E}\right)}{2\left(k + 2\right)\left(1 + k\bar{E}\right)}h, \tag{15b}$$

$$A_t = \left(\bar{E} + \frac{1 - \bar{E}}{k + 1}\right)A, \tag{15c}$$

$$I_e = \frac{bh^3}{12}\left[\bar{E}+12\left(1-\bar{E}\right)\left(\frac{1}{k+3} - \frac{1}{k+2} + \frac{1}{4k+4}\right) - \frac{3k^2\left(1-\bar{E}\right)}{(k+1)(k+2)^2\left(1+k\bar{E}\right)}\right]. \tag{15d}$$

S-FGM:

$$n(z) = \begin{cases} \bar{E} + \dfrac{1}{2}\left(1 - \bar{E}\right)\left(1 + \dfrac{2z}{h}\right)^k & -h/2 \leqslant z \leqslant 0, \\ \bar{E} + \left(1 - \bar{E}\right)\left[1 - \dfrac{1}{2}\left(1 - \dfrac{2z}{h}\right)^k\right] & 0 \leqslant z \leqslant h/2, \end{cases} \tag{16a}$$

$$h_o = \frac{k(k + 3)\left(1 - \bar{E}\right)}{4(k + 1)(k + 2)\left(1 + \bar{E}\right)}h, \tag{16b}$$

$$A_t = \frac{1}{2}\left(1 + \bar{E}\right)A, \tag{16c}$$

$$I_e = \frac{bh^3}{12}\left[\frac{1}{2}\left(1 + \bar{E}\right) - \frac{3k^2(k + 3)^2\left(1 - \bar{E}\right)^2}{8(k + 1)^2(k + 2)^2\left(1 + \bar{E}\right)}\right]. \tag{16d}$$

E-FGM:

$$n(z) = e^{\frac{1}{2}\ln\bar{E}\left(1-\frac{2z}{h}\right)}, \tag{17a}$$

$$h_o = \left[\frac{1 + \bar{E}}{2\left(1 - \bar{E}\right)} + \frac{1}{\ln\bar{E}}\right]h, \tag{17b}$$

$$A_t = \frac{\bar{E} - 1}{\ln\bar{E}}A, \tag{17c}$$

$$I_e = \frac{bh^3}{12}\left[\frac{12\bar{E}\left(\ln\bar{E}\right)^2 - 12\left(1 - \bar{E}\right)^2}{\left(1 - \bar{E}\right)\left(\ln\bar{E}\right)^3}\right]. \tag{17d}$$

Accordingly, the equivalent beam with the transformed cross-section is then considered as a homogeneous beam with an effective bending rigidity $E_t I_e$ and

effective shear rigidity $G_t A_t$ subjected to an eccentric load P_T at a distance $e = h_o - z_T$ from the centroidal axis of the beam. The shear modulus G_t is given by $E_t/2(1+\nu)$ where ν is Poisson's ratio. By applying the minimum potential energy principle and first order shear deformation theory to the equivalent beam with the transformed section under an eccentric load, one can obtain the following static bending equations for the FGM beam under a thermal compressive load at the end supports.

$$\kappa G_t A_t \left(\frac{\mathrm{d}^2 w}{\mathrm{d}x_1^2} - \frac{\mathrm{d}\phi}{\mathrm{d}x_1} \right) - P_T \frac{\mathrm{d}^2 w}{\mathrm{d}x_1^2} = 0, \tag{18a}$$

$$E_t I_e \frac{\mathrm{d}^2 \phi}{\mathrm{d}x_1^2} + \kappa G_t A_t \left(\frac{\mathrm{d}w}{\mathrm{d}x_1} - \phi \right) = 0. \tag{18b}$$

The boundary conditions at $x_1 = 0, l$ are

$$\text{either} \quad \kappa G_t A_t \left(\frac{\mathrm{d}w}{\mathrm{d}x_1} - \phi \right) - P_T \frac{\mathrm{d}w}{\mathrm{d}x_1} = 0 \qquad \text{or} \quad w = 0, \tag{19a}$$

$$\text{either} \quad E_t I_e \frac{\mathrm{d}\phi}{\mathrm{d}x_1} - P_T e = 0 \qquad \text{or} \quad \phi = 0. \tag{19b}$$

Here w and ϕ denote the bending displacement about the neutral axis x_1 and the rotation about they_1 axis, respectively; κ is the shear correction factor taken to be 5/6 throughout this paper. To study the thermal buckling behavior of bifurcation type [18], only the FGM beams with the clamped end supports are investigated. Hence, the boundary conditions at $x_1 = 0, l$ are

$$w = 0, \qquad \phi = 0. \tag{20}$$

From Eq. (18a) and its derivatives, we have

$$\frac{\mathrm{d}\phi}{\mathrm{d}x_1} = \left(1 - \frac{P_T}{\kappa G_t A_t} \right) \frac{\mathrm{d}^2 w}{\mathrm{d}x_1^2}, \tag{21}$$

$$\frac{\mathrm{d}^3 \phi}{\mathrm{d}x_1^3} = \left(1 - \frac{P_T}{\kappa G_t A_t} \right) \frac{\mathrm{d}^4 w}{\mathrm{d}x_1^4}. \tag{22}$$

Substituting Eq. (21) into Eq. (18b) yields

$$\phi = \bar{\beta} \frac{\mathrm{d}^3 w}{\mathrm{d}x_1^3} + \frac{\mathrm{d}w}{\mathrm{d}x_1}, \qquad \bar{\beta} = \frac{E_t I_e}{\kappa G_t A_t} \left(1 - \frac{P_T}{\kappa G_t A_t} \right). \tag{23}$$

Then, differentiating Eq. (18b) and using Eqs. (21) and (22) leads to the following fourth-order differential equation governing the buckling of FGM beams in terms of the bending deflection w

$$\frac{\mathrm{d}^4 w}{\mathrm{d}x_1^4} + \beta^2 \frac{\mathrm{d}^2 w}{\mathrm{d}x_1^2} = 0, \tag{24a}$$

with

$$\beta^2 = \frac{P_T}{E_t I_e \left(1 - \dfrac{P_T}{\kappa G_t A_t}\right)}. \tag{24b}$$

Substituting Eq. (23) into Eq. (20), the clamped boundary conditions can also be rewritten in terms of w as

$$w = 0, \qquad \bar{\beta}\frac{\mathrm{d}^3 w}{\mathrm{d}x_1^3} + \frac{\mathrm{d}w}{\mathrm{d}x_1} = 0. \tag{25}$$

In the next section, the solutions of the thermal buckling temperature for clamped-clamped FGM beams under uniform temperature and nonlinear temperature rises will be derived.

5. Thermal buckling analysis

The general solution for the bending deflection w in Eq. (24) can be given as

$$w(x_1) = C_1 \cos \beta x_1 + C_2 \sin \beta x_1 + C_3 + C_4 x_1 . \tag{26}$$

Here, the constants C_1, C_2, C_3 and C_4 and value of β are determined by properly imposing the restraint conditions of the beam. Introducing the clamped boundary conditions $w(0) = w(l) = 0$ and $\bar{\beta}w'''(0) + w'(0) = \bar{\beta}w'''(l) + w'(l) = 0$ into Eq. (26) yields the following eigenvalue equation

$$\begin{bmatrix} 1 & 0 & 1 & 0 \\ \cos \beta l & \sin \beta l & 1 & l \\ 0 & \beta - \bar{\beta}\beta^3 & 0 & 1 \\ -\left(\beta - \bar{\beta}\beta^3\right) \sin \beta l & \left(\beta - \bar{\beta}\beta^3\right) \cos \beta l & 0 & 1 \end{bmatrix} \begin{Bmatrix} C_1 \\ C_2 \\ C_3 \\ C_4 \end{Bmatrix} = 0. \tag{27}$$

To obtain a nontrivial solution of Eq. (27), the determinant of its coefficient matrix is taken to be zero, which leads to

$$\sin \frac{\beta l}{2} \left[2\left(\beta - \bar{\beta}\beta^3\right) l \cos \frac{\beta l}{2} - 4 \sin \frac{\beta l}{2}\right] = 0. \tag{28}$$

Thus, the smallest critical value $\beta_{cr} l$ satisfying Eq. (28) is 2π. Therefore, the critical thermal buckling load $(P_T)_{cr}$ of the clamped-clamped FGM beam can be obtained from Eq. (24b) as

$$(P_T)_{cr} = \frac{(2\pi)^2 E_t I_e / l^2}{1 + \dfrac{(2\pi)^2 E_t I_e / l^2}{\kappa G_t A_t}}. \tag{29}$$

For the FGM beams under a uniform temperature rise ΔT, the compressive thermal load in Eq. (9) can be obtained as follows.

$$P_T = BE_t\alpha_t A\Delta T, \tag{30}$$

with

$$B = \frac{\left(1-\bar{E}\right)(1-\bar{\alpha})}{2k+1} + \frac{\left(1-\bar{E}\right)\bar{\alpha} + \bar{E}(1-\bar{\alpha})}{k+1} + \bar{E}\bar{\alpha} \qquad \text{(P-FGM)}, \tag{31a}$$

$$B = \frac{1}{2}\left[1 + \bar{E}\bar{\alpha} - \frac{\left(1-\bar{E}\right)(1-\bar{\alpha})}{k+1} + \frac{\left(1-\bar{E}\right)\bar{\alpha} + \bar{E}(1-\bar{\alpha})}{2(2k+1)}\right] \quad \text{(S-FGM)}, \tag{31b}$$

$$B = \frac{1-\bar{E}\bar{\alpha}}{\bar{E}\bar{\alpha}\ln\left(\bar{E}\bar{\alpha}\right)} \qquad \text{(E-FGM)}. \tag{31c}$$

Here $A = bh$, $\bar{E} = E_b/E_t$ and $\bar{\alpha} = \alpha_b/\alpha_t$. Then, using Eq. (30) in Eq. (29), the critical thermal buckling temperature for clamped-clamped FGM beams with temperature-independent material properties under uniform temperature rise can be obtained as

$$\Delta T_{cr}^{UTR} = \frac{1}{B\alpha_t Al^2}\frac{(2\pi)^2 I_e}{1 + \dfrac{(2\pi)^2 E_t I_e/l^2}{\kappa G_t A_t}}. \tag{32}$$

By properly using the coefficient B (Eq. (31)), the area of transformed section A_t (Eqs. (15c), (16c) and (17c)) and effective area moment of inertia I_e (Eqs. (15d), (16d) and (17d)) in Eq. (32), the closed-form solutions of the critical thermal buckling temperature for the clamped-clamped P-FGM, S-FGM and E-FGM beams under uniform temperature rise can be obtained, respectively.

For the FGM beam under nonlinear temperature rise, we can obtain the following associated thermal load for the P-FGM, S-FGM and E-FGM beam by using Eqs. (6)–(8) in Eq. (9), respectively,

$$P_T = C_o E_t\alpha_t A\left(T_b - T_0\right) + CE_t\alpha_t A\Delta T, \tag{33}$$

where the coefficients C_o and C for the respective P-FGM, S-FGM and E-FGM beam are given as follows.

P-FGM beam

$$C_o = \frac{\left(1-\bar{E}\right)(1-\bar{\alpha})}{2k+1} + \frac{\left(1-\bar{E}\right)\bar{\alpha} + \bar{E}(1-\bar{\alpha})}{k+1} + \bar{E}\bar{\alpha}, \tag{34a}$$

$$C = \frac{1}{R_1}\left\{\sum_{j=0}^{n}\frac{\left(-\bar{K}\right)^j}{(jk+1)}\left[\frac{\left(1-\bar{E}\right)(1-\bar{\alpha})}{(j+2)k+2} + \frac{\left(1-\bar{E}\right)\bar{\alpha} + \bar{E}(1-\bar{\alpha})}{(j+1)k+2} + \frac{\bar{E}\bar{\alpha}}{jk+2}\right]\right\}. \tag{34b}$$

S-FGM beam

$$C_o = \frac{1}{2}\left[1 + \bar{E}\bar{\alpha} - \frac{\left(1-\bar{E}\right)(1-\bar{\alpha})}{k+1} + \frac{\left(1-\bar{E}\right)\bar{\alpha} + \bar{E}\,(1-\bar{\alpha})}{2(2k+1)}\right], \tag{35a}$$

$$\begin{aligned} C = {} & \frac{1}{2D_1}\left\{\sum_{j=0}^{n}\frac{\left(-\frac{1}{2}\bar{K}\right)^j}{(jk+1)}\left[\frac{1}{4}\frac{\left(1-\bar{E}\right)(1-\bar{\alpha})}{(j+2)k+2} + \frac{1}{2}\frac{\left(1-\bar{E}\right)\bar{\alpha} + \bar{E}\,(1-\bar{\alpha})}{(j+1)k+2} + \frac{\bar{E}\bar{\alpha}}{jk+2}\right]\right\} \\ & - \frac{1}{2D_3}\left\{\sum_{j=0}^{n}\frac{\left(\frac{1}{2}\bar{K}_1\right)^j}{(jk+1)}\left[\frac{1}{4}\frac{\left(1-\bar{E}\right)(1-\bar{\alpha})}{(j+2)k+2} - \frac{1}{2}\frac{\left(1-\bar{E}\right) + (1-\bar{\alpha})}{(j+1)k+2} + \frac{1}{jk+2}\right]\right\} \\ & + \frac{1}{2}\left[1 - \frac{1}{2}\frac{\left(1-\bar{E}\right) + (1-\bar{\alpha})}{k+1} + \frac{1}{4}\frac{\left(1-\bar{E}\right)(1-\bar{\alpha})}{2k+1}\right]. \end{aligned} \tag{35b}$$

E-FGM beam

$$C_o = \frac{1-\bar{E}\bar{\alpha}}{\bar{E}\bar{\alpha}\ln\left(\bar{E}\bar{\alpha}\right)}, \tag{36a}$$

$$C = \frac{1}{1-K_b/K_t}\left[\frac{\bar{E}\bar{\alpha}K_b/K_t - 1}{\ln\left(\bar{E}\bar{\alpha}K_b/K_t\right)} - \frac{K_b\left(1-\bar{E}\bar{\alpha}\right)}{K_t\bar{E}\bar{\alpha}\ln\left(\bar{E}\bar{\alpha}\right)}\right]. \tag{36b}$$

Introducing Eq. (33) into Eq. (29), the temperature-independent critical thermal buckling temperature for clamped-clamped FGM beams under nonlinear temperature rise can be obtained as

$$\Delta T_{cr}^{NTR} = \frac{(2\pi)^2 I_e}{C\alpha_t A l^2}\left(\frac{1}{1 + \frac{(2\pi)^2 E_t I_e}{\kappa G_t A_t l^2}}\right) - \frac{C_o\,(T_b - T_0)}{C}. \tag{37}$$

Likewise, the closed-form expressions of the temperature-independent critical thermal buckling temperature for the P-FGM, S-FGM and E-FGM beams under nonlinear temperature rise can be determined, respectively, by substituting the associated coefficients C_o and C, area of transformed section A_t and effective area moment of inertia I_e into Eq. (37).

When the temperature-dependent material properties are concerned, an iteration procedure is needed to calculate the thermal buckling temperatures of FGM beams under uniform temperature and nonlinear temperature rises using Eqs. (32) and (37). The detailed process can be found in [16, 26].

6. Results and discussions

Thermal buckling behaviors of various FGM beams made of a ceramic (Si_3N_4) and a metal (SUS304) under uniform and nonlinear temperature rises are investigated. Three types of materials, such as P-FGM, S-FGM and E-FGM models, are considered. The temperature-dependent coefficients of various material properties for Si_3N_4 and SUS304 are given in Table 1 [32]. For simplicity, Poisson's ratio for both materials is assumed to be constant and taken to be 0.3. The solutions of thermal buckling temperature of FGM beams with and without temperature-dependent materials are presented, and denoted as TD solutions and TID solutions, respectively.

Table 1.
Temperature-dependent coefficients of thermal and material properties for Si_3N_4 and SUS304

material	P_0	P_{-1}	P_1	P_2	P_3
Si_3N_4					
E (Pa)	348.43e+9	0	−3.070e-4	2.160e-7	−8.946e-11
α (1/K)	5.8723e-6	0	9.095e-4	0	0
K (W/mK)	13.723	0	−1.032e-3	5.466e-7	−7.876e-11
SUS304					
E (Pa)	201.04e+9	0	3.079e-4	−6.534e-7	0
α (1/K)	12.330e-6	0	8.086e-4	0	0
K (W/mK)	15.379	0	−1.264e-3	2.092e-6	−7.223e-10

6.1. Model verification

First, the thermal buckling of P-FGM beams is considered. Table 2 presents the values of thermal buckling temperature with different values of k for the P-FGM beams with $l/h = 25$ subjected to uniform temperature rise. Both TID and TD solutions are shown and compared with those by other investigators. As can be seen, the present TID solutions agree well with those given in [20, 22, 25]. The TD

Table 2.
Comparison of buckling temperature ΔT_{cr} (K) of P-FGM beams with $l/h = 25$ under UTR

	source	$k = 0$	0.5	1	2	5	10	∞
TID	present	692.85	510.00	458.78	423.62	394.49	376.22	338.02
	Ref. [20]	692.70	509.89	458.68	423.53	394.39	376.14	337.94
	Ref. [22]	693.05	510.14	458.91	423.75	394.61	376.34	338.12
	Ref. [25]	698.95	–	461.82	–	–	376.70	–
TD	present	508.26	399.57	367.39	345.22	326.46	313.65	285.12
	Ref. [20]	508.17	399.50	367.32	345.15	326.40	313.58	285.06

solutions are in excellent agreement with those in [20] as well. In Table 3, the TID and TD solutions of buckling temperature for P-FGM beams of $l/h = 40$ under nonlinear temperature rise with various values of k are given and compared with those in [20, 26]. A good agreement between the present results and the published ones is also observed.

Table 3.
Comparison of buckling temperature ΔT_{cr} (K) for P-FGM beams with $l/h = 40$ under NTR

	source	$k = 0$	0.5	1	2	5	10	∞
TID	present	534.72	421.56	379.20	345.15	312.63	292.87	255.84
	Ref. [20]	536.62	422.18	379.47	345.22	312.64	292.87	255.81
	Ref. [26]	528.40	419.22	378.22	345.16	325.49	305.49	–
TD	present	411.33	377.77	357.86	337.01	310.13	291.36	255.84
	Ref. [20]	412.24	377.96	357.94	337.03	310.12	291.35	255.81
	Ref. [26]	441.00	381.50	352.58	335.09	302.00	281.08	–

In the next, the thermal buckling of S-FGM beams with different thermal loadings is investigated. To the best of authors' knowledge, the results of S-FGM beams are not found in the published literature. The results of P-FGM beam with $k = 1$ are used for the validation because it has the same properties as the corresponding S-FGM beam. Table 4 shows the thermal buckling temperatures for S-FGM beams of $k = 1$ with various slenderness ratios l/h under uniform temperature rise alongside with those of the corresponding P-FGM beams. The present results agree well with those given by other investigators [20, 22, 25]. Table 5 gives the results of buckling temperature of S-FGM and P-FGM beams with $k = 1$ under nonlinear temperature rise. It can be seen that the present results are consistent with those P-FGM results in [20, 26]. As seen in Tables 4 and 5, the present S-FGM results are identical with the present P-FGM results.

Table 4.
Comparison of buckling temperature ΔT_{cr} (K) of S-FGM and P-FGM beams with $k = 1$ under UTR

	source	$l/h = 25$	30	40
TID	S-FGM (present)	458.78	320.15	180.97
	P-FGM (present)	458.78	320.15	180.97
	P-FGM [20]	458.68	–	–
	P-FGM [22]	458.91	–	–
	P-FGM [25]	461.82	322.78	181.70
TD	S-FGM (present)	367.39	270.69	163.06
	P-FGM (present)	367.39	270.69	163.06
	P-FGM [20]	367.32	–	–

It is attributable to the fact that both S-FGM and P-FGM beams have the identical material properties when $k = 1$.

Table 5.
Comparison of buckling temperature ΔT_{cr} (K) of S-FGM and P-FGM beams with $k = 1$ under NTR

	source	$l/h = 25$	30	40
TID	S-FGM (present)	977.94	679.18	379.20
	P-FGM (present)	977.94	679.18	379.20
	P-FGM [20]	–	–	379.47
	P-FGM [26]	–	–	378.22
TD	S-FGM (present)	845.06	613.79	357.86
	P-FGM (present)	845.06	613.79	357.86
	P-FGM [20]	–	–	357.94
	P-FGM [26]	–	–	352.58

6.2. Parametric study

Parametric studies are presented next to investigate the effects of temperature-dependent property, volume fraction index, slenderness ratio and material gradient type on the thermal buckling temperature of FGM beams. Tables 6 and 7 shows the buckling temperatures for P-FGM, S-FGM and E-FGM beams with slenderness ratio $l/h = 30$ under UTR and NTR thermal gradient, respectively. The P-FGM and S-FGM beams are analyzed by varying the value of the volume fraction index. As seen, the TID solutions always give higher values of buckling temperature than the corresponding TD solutions. The comparison between UTR and NTR solutions indicates that the NTR results are significantly greater than the UTR ones for all material types and parameters. It can also be found that both TID and TD solutions reduce with the increasing volume fraction index k for P-FGM beams, while those of S-FGM beams have the opposite tendency.

Table 6.
Buckling temperature ΔT_{cr} (K) of various FGM beams with $l/h = 30$ 30 under UTR

beam		$k = 0$	0.5	1	2	5	10	∞
P-FGM	TID	483.53	355.88	320.15	295.66	275.38	262.63	235.90
	TD	380.23	295.75	270.69	253.22	238.42	228.72	207.80
S-FGM	TID	317.10	318.66	320.15	322.25	325.47	327.54	330.71
	TD	268.63	269.69	270.69	272.13	274.41	275.92	278.27
E-FGM	TID	336.14						
	TD	282.06						

Table 7.

Buckling temperature ΔT_{cr} (K) of various FGM beams with $l/h = 30$ under NTR

beam		$k = 0$	0.5	1	2	5	10	∞
P-FGM	TID	953.62	754.13	679.18	618.74	560.92	525.84	460.27
	TD	649.06	631.77	613.79	590.18	550.97	520.22	460.27
S-FGM	TID	622.07	659.54	679.18	698.59	717.23	725.21	734.10
	TD	549.20	592.48	613.79	632.77	646.85	650.72	652.51
E-FGM	TID	715.34						
	TD	621.38						

Fig. 6 presents the variations of thermal buckling temperature against the slenderness ratio l/h for S-FGM beams with $k = 1$ under UTR and NTR thermal gradient, respectively. Both TID and TD solutions decrease with the increase in the slenderness ratio l/h. However, the difference between the TID and TD solutions becomes smaller as the slenderness ratio $l/h > 50$, especially for the FGM beam under NTR. Thus, the temperature-dependent material properties have a significant impact on the buckling temperature for the beam with a smaller slenderness ratio. The influence becomes minor while the beam has a higher slenderness ratio.

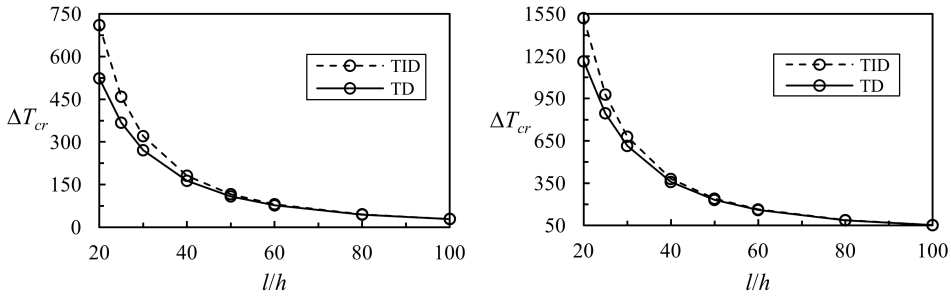

(a) UTR (b) NTR

Fig. 6. Buckling temperature ΔT_{cr} (K) versus l/h for S-FGM beams with $k = 1$

Thermal buckling results for various FGM beams under UTR and NTR thermal condition are given in Figs. 7 and 8, respectively, by changing the slenderness ratio. The P-FGM and S-FGM beams with $k = 0.5$ and 2 are considered, respectively. Similar behaviors regarding the variations of buckling temperature with slenderness ratio l/h for S-FGM beams can also be seen for the P-FGM and E-FGM beams. As observed in Fig. 7a, the P-FGM beam has the highest buckling temperature, followed by the E-FGM beam and S-FGM beam irrespective of the slenderness ratio. In Fig. 7b, it is noted that the E-FGM beam has the greatest buckling temperature, and the P-FGM beam has the least value. As can be found in Fig. 8, the variations of TID solutions under NTR thermal loading against the

different material distribution types show the same tendency as those in the case of UTR thermal loading. However, the TD solutions for different types of FGM beams under NTR thermal loading vary differently depending the slenderness ratio and volume fraction index. As shown in Fig. 8a, the S-FGM beam has the least TD buckling temperature, and the E-FGM beam has the highest TD solution as $l/h = 20$ but the P-FGM beam will have the greatest TD solution when $l/h > 20$. It can be seen in Fig. 8b that the S-FGM beam has the largest TD buckling temperature as $l/h < 50$, but the E-FGM beam has the greatest one as $l/h = 50$, and the P-FGM beam has the smallest value of buckling temperature for each l/h.

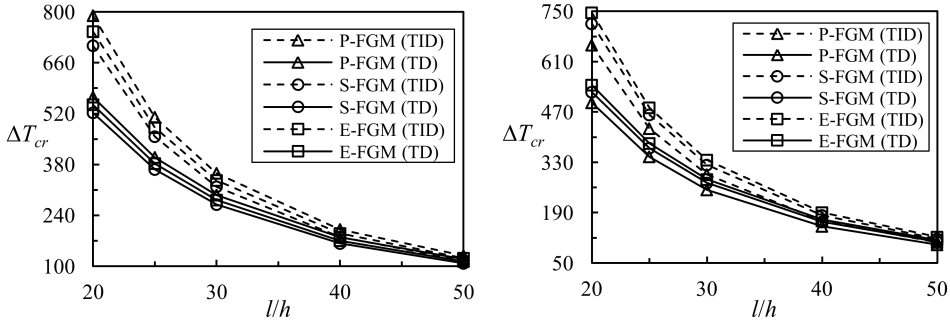

(a) $k = 0.5$ (b) $k = 2$

Fig. 7. Buckling temperature ΔT_{cr} (K) versus l/h for P-FGM, S-FGM and E-FGM beams under UTR

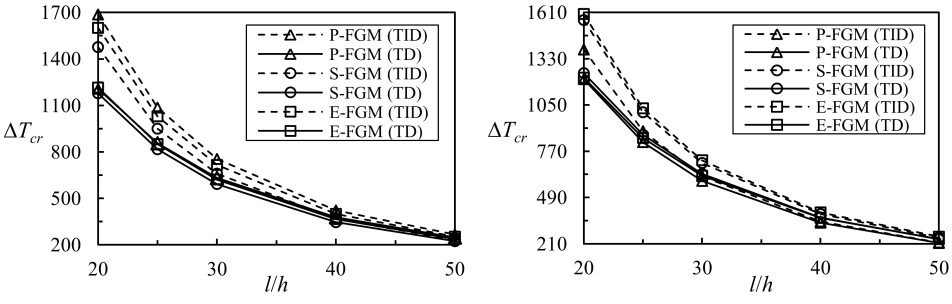

(a) $k = 0.5$ (b) $k = 2$

Fig. 8. Buckling temperature ΔT_{cr} (K) versus l/h for P-FGM, S-FGM and E-FGM beams under NTR

Figs. 9a and 9b illustrate the buckling temperature results against the volume fraction index k for the S-FGM beams with various slenderness ratios under UTR and NTR, respectively. Both the TID and TD solutions increase slightly with the volume fraction index for the beams under UTR irrespective of the slenderness ratio. Unlike the UTR case, both TID and TD solutions for the beams under NTR increase more dramatically as the value of k increases from 0 to 1, but enlarge slightly

thereafter for each slenderness ratio. The considerable effects of temperature-dependent material properties on the buckling temperature are observed for the beams with a small slenderness ratio.

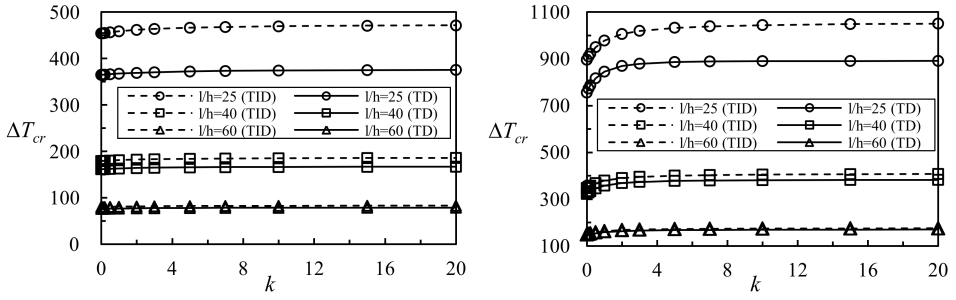

(a) UTR (b) NTR

Fig. 9. Buckling temperature ΔT_{cr} (K) versus k for S-FGM beams with different l/h

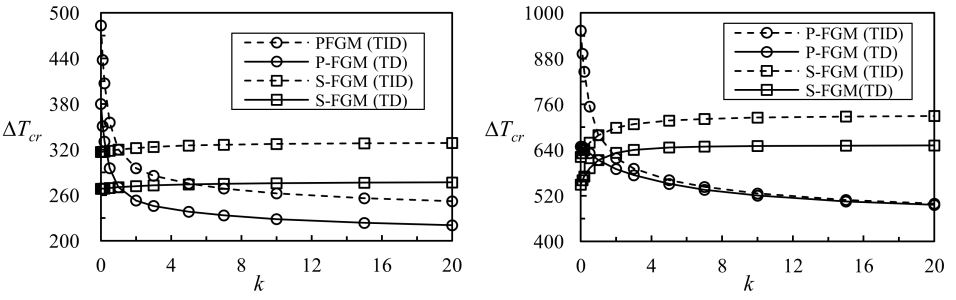

(a) UTR (b) NTR

Fig. 10. Buckling temperature ΔT_{cr} (K) versus k for P-FGM and S-FGM beams with $l/h = 30$

The buckling temperatures resulting from different types of material gradient as P-FGM and S-FGM models are considered with various volume fraction indices, as shown in Fig. 10. The FGM beams with $l/h = 30$ under UTR and NTR thermal loadings are investigated, respectively. Unlike the S-FGM beam, both TID and TD solutions for the P-FGM beam under UTR and NTR reduce sharply with the volume fraction index initially and then decrease gradually. The results in Fig. 10b also indicate that the effects of the temperature-dependent material properties on TD solutions become less significant for P-FGM beams with higher volume fraction index under NTR thermal gradient. As expected, the solutions of the P-FGM and S-FGM beams intersect at the point $k = 1$ where both beams have the identical material properties. It can also be found that the P-FGM beam has the highest buckling temperature as $k < 1$, while the S-FGM beam has the greatest one as $k > 1$. It is due to the fact that the P-FGM beam has the higher volume fraction in ceramic when $k < 1$, while the S-FGM beam is more ceramic-rich as $k > 1$.

7. Conclusions

Thermal buckling behaviors of FGM Timoshenko beams with and without temperature-dependent properties are investigated using the transformed-section method. Three types of material distributions, such as power-law FGM, sigmoid FGM and exponential FGM models are considered. Temperature independent and temperature dependent solutions of the buckling temperature are obtained for the P-FGM, S-FGM and E-FGM beams under uniform and nonlinear temperature rises, respectively. The effects of material gradient type, volume fraction index, slenderness ratio and thermal gradient on the thermal buckling are discussed. Based on the results presented earlier, some major conclusions are addressed as follows.

- The temperature-independent solutions considerably over-estimate the buckling temperature compared to the temperature-dependent solutions, especially for the short FGM beams.
- The buckling temperature of the FGM beam subjected to nonlinear temperature rise is always higher than that under uniform temperature rise.
- The buckling temperature of the FGM beam always reduces with the increasing slenderness ratio regardless of the material gradient types and thermal loadings.
- The buckling temperature of the P-FGM beam decreases, but that of the S-FGM beam increases as the volume fraction index increases.
- The present model provides engineers with a suitable and effective method to analyze the thermal buckling behavior of various FGM Timoshenko beams.

Manuscript received by Editorial Board, August 95, 2019;
final version, October 27, 2019.

References

[1] M. Aydogdu. Semi-inverse method for vibration and buckling of axially functionally graded beams. *Journal of Reinforced Plastics and Composites*, 27(7):683–691, 2008. doi: 10.1177/0731684407081369.

[2] J. Yang and Y. Chen. Free vibration and buckling analyses of functionally graded beams with edge cracks. *Composite Structures*, 83(1):48–60, 2008. doi: 10.1016/j.compstruct.2007.03.006.

[3] A. Shahba, R. Attarnejad, M.T. Marvi, and S. Hajilar. Free vibration and stability analysis of axially functionally graded tapered Timoshenko beams with classic and non-classical boundary conditions. *Composites Part B: Engineering*, 42(4):801–808, 2011. doi: 10.1016/j.compositesb.2011.01.017.

[4] A. Shahba and S. Rajasekaran. Free vibration and stability of tapered Euler-Bernoulli beams made of axially functionally graded materials. *Applied Mathematical Modelling*, 36(7):3094–3111, 2012. doi: 10.1016/j.apm.2011.09.073.

[5] T.K. Nguyen, T.P. Vo, and H.T. Thai. Static and free vibration of axially loaded functionally graded beams based on the first-order shear deformation theory. *Composites Part B: Engineering*, 55:147–157, 2013. doi: 10.1016/j.compositesb.2013.06.011.

[6] S.R. Li and R.C. Batra. Relations between buckling loads of functionally graded Timoshenko and homogeneous Euler-Bernoulli beams. *Composite Structures*, 95:5–9, 2013. doi: 10.1016/j.compstruct.2012.07.027.

[7] J. Rychlewska. Buckling analysis of axially functionally graded beams. *Journal of Applied Mathematics and Computational Mechanics*, 13(4):103–108, 2014.

[8] S.R. Li, X. Wang, and Z. Wan. Classical and homogenized expressions for buckling solutions of functionally graded material Levinson beams. *Acta Mechanica Solida Sinica*, 28(5):592–604, 2015. doi: 10.1016/S0894-9166(15)30052-5.

[9] M.E. Torki and J.N. Reddy. Buckling of functionally-graded beams with partially delaminated piezoelectric layers. *International Journal of Structural Stability and Dynamics*, 16(3):1450104, 2016. doi: 10.1142/S0219455414501041.

[10] B. Shvartsman and J. Majak. Numerical method for stability analysis of functionally graded beams on elastic foundation. *Applied Mathematical Modelling*, 40(5-6):3713–3719, 2016. doi: 10.1016/j.apm.2015.09.060.

[11] Y. Huang, M. Zhang, and H.W. Rong. Buckling analysis of axially functionally graded and non-uniform beams based on Timoshenko theory. *Acta Mechanica Solida Sinica*, 29(2):200–207, 2016. doi: 10.1016/S0894-9166(16)30108-2.

[12] V. Kahya and M. Turan. Finite element model for vibration and buckling of functionally graded beams based on the first-order shear deformation theory. *Composites Part B: Engineering*, 109:108–115, 2017. doi: 10.1016/j.compositesb.2016.10.039.

[13] H. Deng, K. Chen, W. Cheng, and S.G. Zhao. Vibration and buckling analysis of double-functionally graded Timoshenko beam system on Winkler-Pasternak elastic foundation. *Composite Structures*, 160:152–168, 2017. doi: 10.1016/j.compstruct.2016.10.027.

[14] V. Kahya and M. Turan. Vibration and stability analysis of functionally graded sandwich beams by a multi-layer finite element. *Composites Part B: Engineering*, 146:198–212, 2018. doi: 10.1016/j.compositesb.2015.02.032.

[15] Y. Kiani and M.R. Eslami. Thermal buckling analysis of functionally graded materials beams. *International Journal of Mechanics and Materials in Design*, 6(3):229–238, 2010. doi: 10.1007/s10999-010-9132-4.

[16] N. Wattanasakulpong, B. Gangadhara Prusty, and D.W. Kelly. Thermal buckling and elastic vibration of third-order shear deformable functionally graded beams. *International Journal of Mechanical Sciences*, 53(9):734–743, 2011. doi: 10.1016/j.ijmecsci.2011.06.005.

[17] A. Fallah and M.M. Aghdam. Thermo-mechanical buckling and nonlinear free vibration analysis of functionally graded beams on nonlinear elastic foundation. *Composites Part B: Engineering*, 43(3):1523–1530, 2012. doi: 10.1016/j.compositesb.2011.08.041.

[18] Y. Kiani and M.R. Eslami. Thermomechanical buckling of temperature-dependent FGM beams. *Latin American Journal of Solids and Structures*, 10(2):223–245, 2013. doi: 10.1590/S1679-78252013000200001.

[19] Y. Fu, Y. Chen, and P. Zhang. Thermal buckling analysis of functionally graded beam with longitudinal crack. *Meccanica*, 48(5):1227–1237, 2013. doi: 10.1007/s11012-012-9663-x.

[20] S.E. Esfahani, Y. Kiani, and M.R. Eslami. Non-linear thermal stability analysis of temperature dependent FGM beams supported on non-linear hardening elastic foundations. *International Journal of Mechanical Sciences*, 69:10–20, 2013. doi: 10.1016/j.ijmecsci.2013.01.007.

[21] L.C. Trinh, T.P. Vo, H.T. Thai, and T.K. Nguyen. An analytical method for the vibration and buckling of functionally graded beams under mechanical and thermal loads. *Composites Part B: Engineering*, 100:152–163, 2016. doi: 10.1016/j.compositesb.2016.06.067.

[22] Y. Sun, S.R. Li, and R.C. Batra. Thermal buckling and post-buckling of FGM Timoshenko beams on nonlinear elastic foundation. *Journal of Thermal Stresses*, 39(1):11–26, 2016. doi: 10.1080/01495739.2015.1120627.

[23] T.K. Nguyen, B.D. Nguyen, T.P. Vo, and H.T. Thai. Hygro-thermal effects on vibration and thermal buckling behaviours of functionally graded beams. *Composite Structures*, 176:1050–1060, 2017. doi: 10.1016/j.compstruct.2017.06.036.

[24] G.L. She, F.G. Yuan, and Y.R. Ren. Thermal buckling and post-buckling analysis of functionally graded beams based on a general higher-order shear deformation theory. *Applied Mathematical Modelling*, 47:340–357, 2017. doi: 10.1016/j.apm.2017.03.014.

[25] M. Hosseini, F. Farhatnia, and S. Oveissi. Functionally graded Timoshenko beams with elastically-restrained edge supports: thermal buckling analysis via Stokes' transformation technique. *Research on Engineering Structures and Materials*, 4(2):103–125, 2018. doi: 10.17515/resm2016.83me1018.

[26] A. Majumdar and D. Das. A study on thermal buckling load of clamped functionally graded beams under linear and nonlinear thermal gradient across thickness. *Proceedings of the Institution of Mechanical Engineers, Part L: Journal of Materials: Design and Applications*, 232(9):769–784, 2018. doi: 10.1177/1464420716649213.

[27] Y. Liu, S. Su, H. Huang, and Y. Liang. Thermal-mechanical coupling buckling analysis of porous functionally graded sandwich beams based on physical neutral plane. *Composites Part B: Engineering*, 168:236–242, 2019. doi: 10.1016/j.compositesb.2018.12.063.

[28] A.C. Ugural. *Mechanical Design: An Integrated Approach*. McGraw-Hill Company, Singapore, 2004.

[29] W.R. Chen and H. Chang. Closed-form solutions for free vibration frequencies of functionally graded Euler-Bernoulli beams. *Mechanics of Composite Materials*, 53(1):79–98, 2017. doi: 10.1007/s11029-017-9642-3.

[30] W.R. Chen and H. Chang. Vibration analysis of functionally graded Timoshenko beams. *International Journal of Structural Stability and Dynamics*, 18(1):1850007, 2018. doi: 10.1142/S0219455418500074.

[31] Y.S. Touloukian. *Thermophysical Properties of High Temperature Solids Materials*. MacMillan, New York, 1967.

[32] J.N. Reddy and C.D. Chin. Thermomechanical analysis of functionally graded cylinders and plates. *Journal of Thermal Stresses*, 21(6):593–626, 1998. doi: 10.1080/01495739808956165.